Microwave-Based Quantum Control and Coherence Protection of Tin-Vacancy Spin Qubits in a Strain-Tuned Diamond-Membrane Heterostructure

Guo, Xinghan; Stramma, Alexander M.; Li, Zixi; Roth, William G.; Huang, Benchen; Jin, Yu; Parker, Ryan A.; Arjona Martínez, Jesús; Pingault, Benjamin; More Authors

DOI
10.1103/PhysRevX.13.041037

Publication date
2023

Document Version
Final published version

Published in
Physical Review X

Microwave-Based Quantum Control and Coherence Protection of Tin-Vacancy Spin Qubits in a Strain-Tuned Diamond-Membrane Heterostructure

Xinghan Guo,[1,‡] Alexander M. Stramma,[2,‡] Zixi Li,[1] William G. Roth,[2] Benchen Huang,[3] Yu Jin,[3] Ryan A. Parker,[2] Jesús Arjona Martínez,[2] Noah Shofer,[2] Cathryn P. Michaels,[2] Carola P. Purser,[2] Martin H. Appel,[2] Evgeny M. Alexeev,[2,4] Tianle Liu,[5] Andrea C. Ferrari,[4] David D. Awschalom,[1,5,6] Nazar Delegan,[1,6] Benjamin Pingault,[6,7] Giulia Galli,[1,3,6] F. Joseph Heremans,[1,6] Mete Atatüre,[2,*] and Alexander A. High[1,6,†]

[1]*Pritzker School of Molecular Engineering, University of Chicago, Chicago, Illinois 60637, USA*
[2]*Cavendish Laboratory, University of Cambridge, Cambridge CB3 0HE, United Kingdom*
[3]*Department of Chemistry, University of Chicago, Chicago, Illinois 60637, USA*
[4]*Cambridge Graphene Centre, University of Cambridge, Cambridge CB3 0FA, United Kingdom*
[5]*Department of Physics, University of Chicago, Chicago, Illinois 60637, USA*
[6]*Center for Molecular Engineering and Materials Science Division, Argonne National Laboratory, Lemont, Illinois 60439, USA*
[7]*QuTech, Delft University of Technology, 2600 GA Delft, Netherlands*

(Received 21 July 2023; revised 25 August 2023; accepted 22 September 2023; published 29 November 2023)

Robust spin-photon interfaces in solids are essential components in quantum networking and sensing technologies. Ideally, these interfaces combine a long-lived spin memory, coherent optical transitions, fast and high-fidelity spin manipulation, and straightforward device integration and scaling. The tin-vacancy center (SnV) in diamond is a promising spin-photon interface with desirable optical and spin properties at 1.7 K. However, the SnV spin lacks efficient microwave control, and its spin coherence degrades with higher temperature. In this work, we introduce a new platform that overcomes these challenges—SnV centers in uniformly strained thin diamond membranes. The controlled generation of crystal strain introduces orbital mixing that allows microwave control of the spin state with 99.36(9)% gate fidelity and spin coherence protection beyond a millisecond. Moreover, the presence of crystal strain suppresses temperature-dependent dephasing processes, leading to a considerable improvement of the coherence time up to 223(10) μs at 4 K, a widely accessible temperature in common cryogenic systems. Critically, the coherence of optical transitions is unaffected by the elevated temperature, exhibiting nearly lifetime-limited optical linewidths. Combined with the compatibility of diamond membranes with device integration, the demonstrated platform is an ideal spin-photon interface for future quantum technologies.

DOI: 10.1103/PhysRevX.13.041037

Subject Areas: Condensed Matter Physics, Quantum Physics, Quantum Information

I. INTRODUCTION

Color centers in diamond are a leading platform in quantum technologies, key achievements such as the demonstration of a quantum register [1–3], distant entanglement generation between three nodes [4], quantum teleportation [5], along with myriad landmarks in quantum sensing [6,7]. In recent years, group IV centers have gained much attention due to their excellent optical properties [8–15]. Their D_{3d} symmetry renders optical transitions insensitive to first-order charge noise [16–18]. Additionally, a favorable Debye-Waller factor leads to the majority of photons being emitted into the zero-phonon line, critical for spin-photon entanglement [19]. However, the electronic structure of group IV centers—a spin-1/2 system with two ground-state orbital branches—renders the electron spin susceptible to phonon-driven transitions between the two branches [20]. This temperature-dependent spin dephasing can be mitigated by operating at millikelvin temperatures [21,22] or by engineering the local phonon density of states through nanostructuring [23,24]. Alternatively, dephasing can be mitigated by qubit engineering such as working with group IV centers with high

*To whom all correspondence should be addressed: ma424@cam.ac.uk

†To whom all correspondence should be addressed: ahigh@uchicago.edu

‡These authors contributed equally to this work.

spin-orbit coupling and, thus, large orbital splitting [25] or by leveraging spin-strain interaction in randomly or controllably strained group IV centers [3,24]. With a spin-orbit coupling significantly higher than those of the silicon-vacancy (SiV) and the germanium-vacancy (GeV) centers, the SnV center has the highest reported spin coherence time at 1.7 K [26]. However, efficient microwave (MW) control of group IV spins requires the magnitude of spin-strain interaction to be comparable with the spin-orbit interaction, which for SnV necessitates strain approaching 0.1%. This degree of strain is challenging to achieve in microelectrical mechanical structures (MEMS) such as diamond cantilevers, with reported values on the order of 0.015% [23]. Therefore, a controlled process to generate approximately 0.1% strain in diamond is desired to improve SnV qubit performance by both increasing the operational temperature and enabling efficient MW driving.

In this work, we utilize heterogeneous integration of diamond membranes to generate strain-tuned SnVs. By bonding SnV-incorporated pristine diamond membranes to a glass substrate, we leverage the heterogeneous thermal expansion coefficients of the two materials to generate a uniform, in-plane strain in the diamond to the order of 0.1%. This strain greatly increases the energy splitting between the two orbital levels of the SnV and induces orbital mixing in the spin ground state. We demonstrate MW manipulation of the spin with 99.36(9)% Rabi fidelity at 4.50(2) MHz for 24 dBm MW input power. At 1.7 K, the implementation of dynamical decoupling allows the SnV to reach millisecond coherence time, which is largely preserved even at 4 K, owing to the strain-induced increased ground-state orbital splitting. In combination with near lifetime-limited optical linewidths up to 7 K, our spin-photon interface is compatible with broadly utilized low-infrastructure and cost-effective portable cryogenic systems. Additionally, the demonstrated strained-membrane heterostructure maintains robustness and flexibility for additional photonic, electronic, and MEMS integration. Our SnV-based diamond-membrane platform greatly reduces the technological barrier for establishing quantum nodes for networking.

A. SnVs in strained diamond

This work relies on strain engineering to improve SnV qubit performance. First, we demonstrate that heterogeneous thermal expansion disparities between diamond and glass in a diamond-membrane heterostructure are sufficient to generate uniform strain of the magnitude necessary to beneficially impact SnV. The diamond membranes used in this work are generated via the "smart-cut" method combined with isotopically purified (^{12}C) overgrowth. The membrane thickness is nominally 150 nm, with pristine crystal quality and atomically smooth surfaces [27]. To introduce a positive tensile strain inside the diamond membrane, we bond them onto 500-μm-thick fused silica substrates—a material with a low thermal expansion coefficient ($< 1 \times 10^{-6}$ K^{-1})—using a layer of hydrogen silsesquioxane (HSQ). The schematic of this strain generation method is shown in Fig. 1(a). The device is then annealed at 600 °C, beyond the temperature at which the HSQ solidifies to glass, bonding the heterostructure in a "zero-strain" condition [28]. Because of the mismatch in thermal contraction between diamond and fused silica and the negligible thickness of the diamond membrane compared to that of the fused silica substrate, cooling down the device to cryogenic temperature regime generates a positive (tensile), static strain profile in the diamond membrane with an estimated magnitude of 0.05% to 0.1% (see Secs. I. 3 and I. 4 in Supplemental Material [29] for details). This passive, uniform, and membrane-compatible strain generation is complementary to recent demonstrations of electromechanically induced strain on suspended diamond beams [24,30].

Figure 1(b) is the microscope image showing the layout of our diamond-membrane heterostructure device. Prior to the membrane bonding, we pattern and etch a 5-μm-deep trench on the fused silica to suspend part of the membrane and mitigate background fluorescence from the HSQ resist. To study MW control of the SnV centers, we pattern and deposit gold coplanar waveguides following membrane bonding.

The strain monotonically increases the orbital splitting of the SnV centers in the membranes, which can be directly verified in the photoluminescence (PL) spectra at 1.7 K. The energy level diagram of the strained SnV is shown in Fig. 1(c), highlighting the ground-state orbital splitting (Δ_{gs}) and the respective contributions of spin-orbit coupling, strain, and magnetic Zeeman interaction in purple, blue, and green boxes, respectively. Figure 1(d) compares the spectra of a strained (unstrained) SnV center in a diamond membrane (bulk diamond) with $\Delta_{gs} = \approx 1300(850)$ GHz. This particular strained center is used in further optical, microwave, and spin characterizations in this work. Remarkably, we note that all color centers in the membrane are comparably strained. As shown in Fig. 1(e), we observe a distribution of the orbital branches splitting centered around 1500 GHz across different devices with a minimum (maximum) value of 1200 (1800) GHz. We carry out density functional theory calculations to compute strain susceptibilities and characterize the SnV spin-strain interaction (see Supplemental Material [29]); our results show that the increase of the splitting between orbital branches from 850 GHz to approximately 1500 GHz due to strain corresponds to a diamond-membrane strain magnitude of 0.075% (see Sec. I. 2 in Supplemental Material [29] for details). The consistent strain generation, in combination with our ability to perform additional integration and nanofabrication following membrane bonding [31,32], highlights the robustness and versatility of our platform.

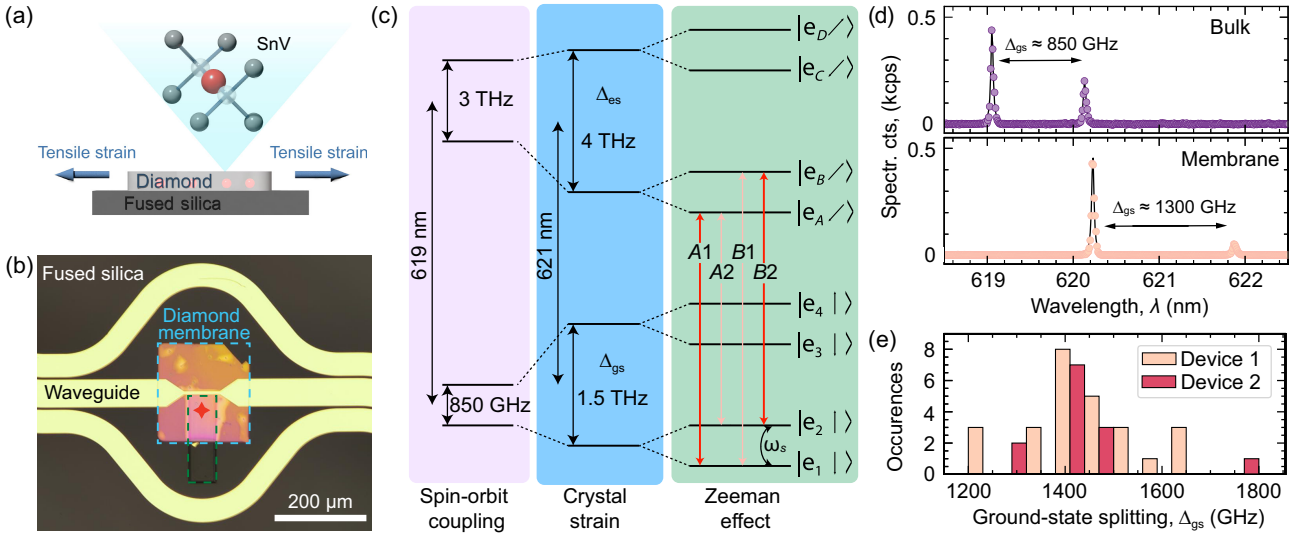

FIG. 1. Strained SnV in diamond-membrane heterostructures. (a) Schematics of the diamond-fused silica heterostructure. The static, tensile strain inside the membrane is generated from the disparity of thermal expansion ratios of diamond and fused silica. (b) The microscope image of the diamond membrane (dashed cyan region) bonded to the fused silica substrate. A trench (dashed green region) is fabricated prior to bonding. The gold coplanar waveguide is fabricated postbonding to introduce microwave signals. The location of the SnV center used in this study is highlighted by a red star. (c) Energy level of strained SnVs. Unstrained centers, strained centers, and strained centers in the presence of a magnetic field are colored in purple, blue, and green, respectively. (d) The PL spectrum of a strained SnV center (orange), showing a redshifted zero-phonon line (ZPL) wavelength with a much larger ground-state splitting compared with the values in bulk diamond (purple). (e) The statistics of the SnV ground-state splitting. Two different devices with identical layout are measured. Device 1 (orange) is used for all-optical spin control (discussed in Supplemental Material [29]), and device 2 (purple) is used for microwave spin control.

B. Optical properties of SnV under strain

To investigate the potential of strained SnV as a spin-photon interface, we first verify that the symmetry of the defect is preserved even under considerable strain by characterizing the optical transitions as a function of the magnetic (B) field orientation. Using the $\langle 111 \rangle$ crystallographic axis—the high-symmetry axis of the SnV—as the reference, we rotate the B field in both polar (θ) and azimuthal (ϕ) angles at the same magnitude (0.2 T). The absolute energy splitting between the two spin-conserving transitions ($A1$-$B2$) with respect to θ and ϕ is shown in Fig. 2(a), indicating that large splittings at moderate values of magnetic field are achievable which is ideal for later SnV spin initialization and control. Similarly to the unstrained case, we observe a ϕ rotational symmetry of the splitting with respect to $\langle 111 \rangle$, which corresponds to the intrinsic spin quantization axis. We further verify that the polarization of the SnV transitions (i.e., dipole operator matrix elements) remain along the $\langle 111 \rangle$ direction (see Sec. III. 1 in Supplemental Material [29]), as in the unstrained case [18].

From the B-field scan of the strained SnV, we note that, besides the normal $A1$-$B2$ splitting maximum along the quantization axis, an additional local maximum at $\theta = 90°$—the equator plane perpendicular to the quantization axis—is observed, with the relative $A1$-$B2$ position being inverted, as verified by coherent population trapping

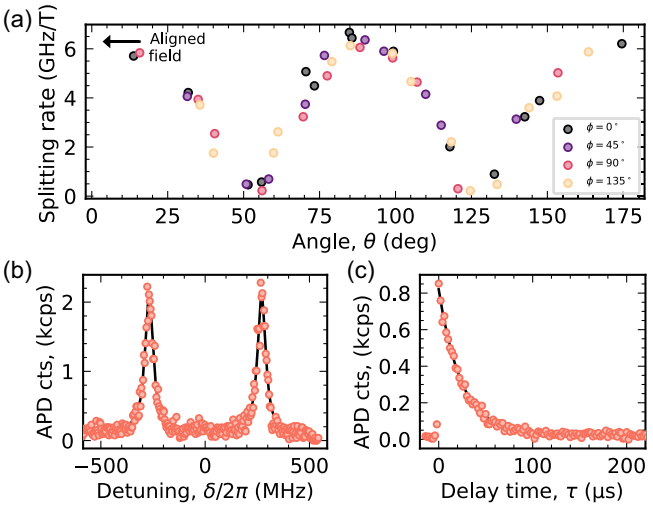

FIG. 2. Optical properties of the strained SnV center under applied magnetic fields at 1.7 K. (a) The energy splitting rate between the $A1$-$B2$ spin-conserving transitions with respect to the polar angle θ of the applied magnetic field at different azimuthal angles ϕ. The aligned field is highlighted with a black arrow. (b) Photoluminescence excitation scan, averaged over 20 s, of the $\{A1, B2\}$ transitions at an aligned B field with a magnitude of 81.5 mT. The average linewidth for both transitions is below 48 MHz, which is less than 1.5 times of the lifetime-limited value [32.26(19) MHz]. (c) The initialization curve of the $A1$ transition, showing a time constant of 24.2(3) μs and an initialization fidelity of 98.82%.

measurements (see Supplemental Material [29]). This differs from the unstrained case. The novel feature arises from the moderate crystal strain (comparable in magnitude to the spin-orbit coupling) which increases the difference in effective Zeeman shift between ground and excited states, mostly visible for a magnetic field orthogonal to the xspin-orbit-dictated quantization axis. As is the case for moderately strained SiV centers [22] for MW-based control, we roughly align the B field toward the quantization axis to achieve highly cycling optical transitions with cyclicity reaching $\eta \approx 2500$ (see Sec. IV. 2 in Supplemental Material [29]). We note that η can be as low as 6 when the B field is perpendicular to the quantization axis, which is ideal for Raman-based all-optical control of strained SnV (see Sec. IV. 3 in Supplemental Material [29]). Moreover, by comparing the dependence on θ of the $A1$-$B2$ splitting with calculated results, we are able to determine the Stevens reduction factor g_L for ground and excited states mentioned in Ref. [33]. This model is then used to explain the optically detected magnetic resonance (ODMR) frequency of the strained SnV discussed below.

Additionally, our measurements reveal near-transform-limited optical linewidths, thereby showing that the application of strain does not alter the excellent coherence properties of the optical transitions, as previously demonstrated with unstrained centers [11,25]. As shown in Fig. 2(b), the 20 s average scan returns a mean linewidth of 47.4(16) MHz, only 40% more than the lifetime-limited value of 32.26(19) MHz [4.933(190) ns optical lifetime; see Sec. III. 2 in Supplemental Material [29]]. The long-term frequency stability of the $\{A1, B2\}$ transitions returns a center frequency standard deviation of $\sigma_c = 23.8(1)$ MHz and an $A1$-$B2$ splitting standard deviation of $\sigma_s = 13.28(6)$ MHz (see Sec. III. 4 in Supplemental Material [29]). This linewidth and peak stability is comparable to that of other measurements of group IV color centers in nanostructures [3,13,34] and, thus, confirms the excellent potential of these defects for quantum photonic applications.

The resolvable splitting and narrow optical transitions are crucial for the spin initialization and readout of the SnV qubit. The spin initialization curve with subtracted background is shown in Fig. 2(c), indicating a fitted exponential decay constant of 24.2(3) μs. The initialization pulse duration is set to 200 μs, allowing us to reach a fidelity of 98.8%. We note that, with a cyclicity of over 2500, this platform is a prime candidate for single-shot readout if the signal counts can be improved via on-chip structures (nanophotonics, fiber couplers or grating couplers, solid immersion lenses) [34–39] or external methods (microcavities) [40–42].

C. Efficient MW control of the SnV spin

A critical component of a spin-photon interface is high-fidelity spin control, commonly achieved through MW driving of the electron spin. In the case of group IV centers, a MW field can drive the spin transition only in the presence of strain [23,43]. This arises due to the orthogonality of orbital states associated with the electron spin qubit of group IV centers [18]. Strain that is comparable in strength to spin-orbit coupling relaxes this orthogonality, enabling microwave control. SnV, with larger spin-orbit coupling (850 GHz) and smaller strain susceptibility than SiV and GeV, requires large crystal strain to meet this criteria. This strain requirement goes beyond the achievable magnitude demonstrated via active strain tuning [23] or implantation-induced strain [3].

To demonstrate efficient MW control, we utilize the nominal 0.1% crystal strain in the diamond membrane. We estimate an effective Landé factor g of 1.62 for the transverse microwave field with the external magnetic field roughly aligned to the SnV quantization axis (see Sec. II. 1 in Supplemental Material [29]). This value is relatively high compared with the spin-orbit-dominated regime for unstrained centers (≤ 0.3) and is close to the free electron value ($g = 2$). In addition, we taper the MW waveguide around the measurement area by shrinking its width to 6 μm to enhance the microwave amplitude, as shown in Fig. 1(b). The distance between the target SnV and the waveguide is approximately 4 μm, ensuring an efficient exposure to the MW driving field (see Secs. 2.1–2.3 in Supplemental Material [29] for details).

We begin the MW control characterization by initializing the spin via optical pumping and scan the frequency of a MW field across the expected spin resonance while monitoring the fluorescence intensity of the spin readout at 1.7 K. In Fig. 3(a), we observe a clear signature of ODMR for the target SnV center. The 81.5 mT external magnetic field is aligned to the quantization axis by polarization measurements and 3D field scan. The ODMR shows a profile with two overlapping peaks separated by 628(182) kHz, indicating an interaction between the electronic spin of the SnV with another system in the vicinity, likely a [^{13}C] nuclear spin or the electron spin of a $P1$ center. Further investigation is needed to understand the nature of this interaction. By driving both power-broadened ODMR transitions, we are able to resonantly manipulate the spin state of the SnV with a Rabi frequency $\Omega/2\pi$ of 4.50(2) MHz. The Rabi oscillation curve and the chevrons (Rabi oscillations with varied driving frequency) are shown in Figs. 3(b) and 3(c). We observe a long-time averaged Rabi π-gate fidelity of 99.36(9)%, improving significantly from a previously demonstrated optical Raman-based spin control value [26]. We note that the MW power delivered to the device is approximately 24 dBm (250 mW) which is comparable to previous demonstrations on strained SiV [3]. We also characterize the power dependence of the Rabi rate. Starting from a linear dependence, the Rabi rate deviates to sublinear when the power surpasses 24 dBm due to excessive heating (see Sec. II. 4 in Supplemental Material [29]), which could be

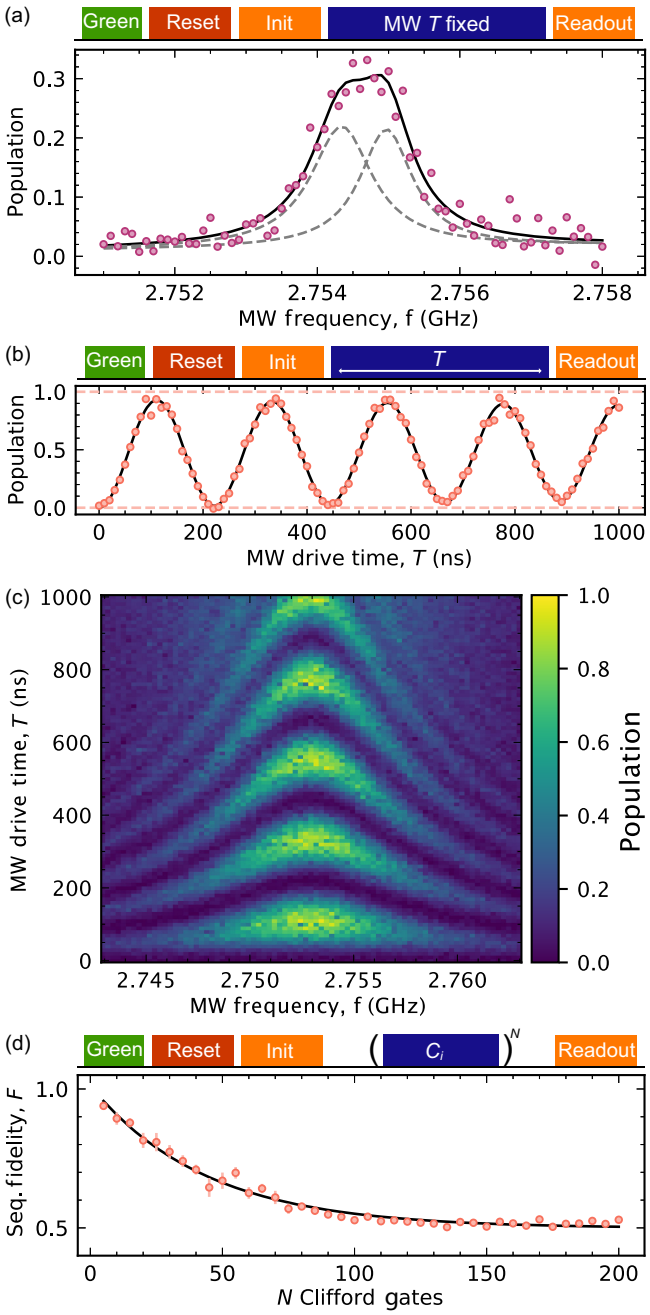

FIG. 3. MW control of the strained SnV center at 1.7 K. (a) Pulsed ODMR spectrum with scanned MW frequency. The data (purple dots) are fitted with two Lorentzian functions (dashed line) split by 628(182) kHz and with a linewidth of 1047(208) and 891(197) kHz, respectively. (b) Rabi oscillation of the SnV at zero detuning, indicating a Rabi frequency $\Omega/2\pi$ of 4.50(2) MHZ with a fidelity of 99.36(9)%. (c) Rabi oscillation as a function of the MW driving frequency. (d) Randomized benchmarking at 1.7 K, showing an average gate fidelity of 97.7(1)%. The Rabi frequency is set to 2.8 MHZ to avoid excess heating effects.

optimized by replacing gold with superconducting metals (such as niobium or NbTiN) to deliver the MW signal.

We further characterize the single-qubit gate fidelity of MW control via randomized benchmarking. For this, we use the following set of Clifford gates: $\{I, \pi_x, \pi_y, \pi_x/2, -\pi_x/2, \pi_y/2, -\pi_y/2\}$ (see Sec. V. 1 in Supplemental Material [29]). To prevent excessive heating effect during benchmarking which would lead to undesired spin decoherence, we apply a slightly slower Rabi rate (2.8 MHz, 18 dBm) which requires no time buffer between gates. The benchmarking result is shown in Fig. 3(d). We extract an average Clifford gate fidelity of 97.7(1)%, indicating power-efficient MW control with high fidelity under stringent randomized benchmarking.

D. SnV spin coherence properties

We next utilize microwave control to characterize the SnV coherence at 1.7 K. We perform a Ramsey measurement as shown in Fig. 4(a). The Gaussian envelope of the Ramsey oscillations corresponds to a spin dephasing time T_2^* of 2.5(1) μs. Similar to ODMR, we observe interaction with a proximal spin in the Ramsey measurement, and we verify that this does not originate from the detuning of the MW signal via phase-dependent readout (see Sec. V. 2 in Supplemental Material [29]). Possible decoherence sources could be nearby vacancies and defects in the diamond membrane, as well as surface spins from both sides of the membrane [44].

Advanced pulse sequences, such as dynamical decoupling via Carr-Purcell-Meiboom-Gill (CPMG) and XY pulse sequences [45,46], allow us to extend the spin

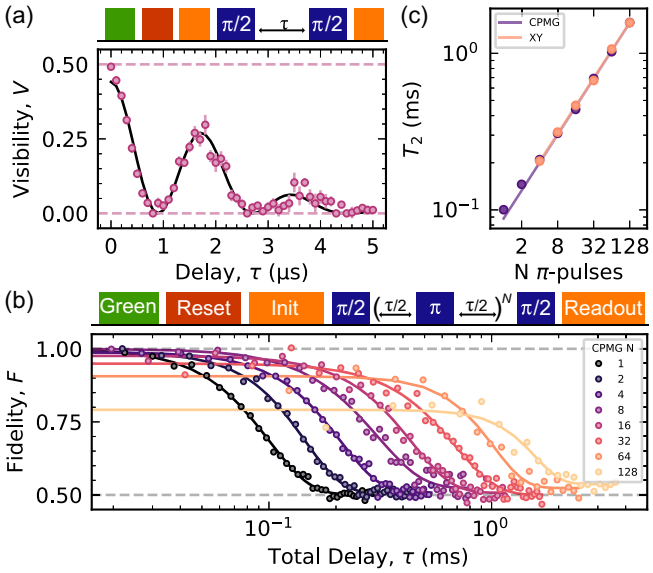

FIG. 4. Spin coherence of the strained SnV at 1.7 K. (a) T_2^* Ramsey of the SnV center, showing a dephasing time of 2.5(1) μs. The extra beating pattern of 554(5) kHz is estimated to be an interaction with the electron or nuclear spin in the vicinity. (b) Dynamical decoupling of the SnV via CPMG pulses. The CPMG-1 (spin echo) returns a $T_{2,\mathrm{echo}}$ of 100(1) μs, while the CPMG-128 reaches a $T_{2,\mathrm{CPMG128}}$ of 1.57(8) ms. (c) The scaling of T_2 with the number of CPMG and XY pulses, showing a sublinear dependence.

coherence to millisecond timescales. The CPMG results are shown in Fig. 4(b). The $T_{2,\mathrm{echo}}$ returns a value of 100(1) μs, which is already longer than 35.5(30) μs measured using all-optical spin echo process (see Secs. 4.3 and 4.4 in Supplemental Material [29]), in the absence of optically induced dephasing mechanisms. The $T_{2,\mathrm{CPMG128}}$, comprising 128 refocusing microwave pulses, prolongs the SnV spin coherence to 1.57(8) ms. We note that, with no signal normalization being applied, the CPMG figure indicates a high signal fidelity of approximately 80% for up to 128 pulses. Future developments on the MW driving fidelity including superconducting metals and faster Rabi pulses can further improve the signal fidelity to higher numbers of pulses. We plot the relationship between the T_2 and the number of CPMG or XY pulses N in Fig. 4(c) and fit it with $T_2 \sim N^{\beta}$. The fitting curve returns a sublinear dependence with a β factor of 0.593(8). We observe minimal T_2 differences between CPMG and XY sequences. XY sequences are more resilient to control pulse errors compared to CPMG [46], verifying that the observed coherence is not limited by our control (see Sec. V. 4 in Supplemental Material [29]).

E. Spin-photon interface at 4 K

Finally, we demonstrate that our strained SnV platform shows state-of-the-art spin coherence for group IV color centers at 4 K. For group IVs, the dominant decoherence source of the electronic spin is the electron-phonon interaction (phonon-mediated decay) between orbital branches [20,43]. The electron-phonon interaction rate depends on the temperature-dependent phonon population and the energy splitting Δ_{gs} between orbital branches. Therefore, enhanced coherence of the group IV centers can be achieved via either cooling down to millikelvin temperature [21,22], increased energy splitting by using heavier group IV elements [25], engineering of the phonon density of states [47], or strain engineering [24]. Here, we utilize both a heavy element (Sn as compared to Si and Ge) and crystal strain in diamond to improve electron spin coherence at elevated temperatures.

The Rabi oscillation of the SnV at 4 K is shown in Fig. 5(a). The fidelity is characterized to be 97.7(5)%, only slightly lower than the value at 1.7 K due to background heating limitations. We characterize the average gate fidelity via randomized benchmarking at 4 K using the same 2.8 MHz Rabi rate, returning a gate fidelity of 95.7 (3)%, confirming the maintained high-performance spin manipulation of the strained SnV at 4 K.

Equipped with high-fidelity Rabi control, we investigate the spin coherence of the SnV centers at elevated temperatures. Because of the much larger splitting Δ_{gs} of the strained SnV (approximately 1300 GHz) compared with bulk SnV (approximately 850 GHz), electron-phonon dephasing onsets at higher temperatures. Figure 5(c) shows the T_1^{spin}, T_2^*, $T_{2,\mathrm{echo}}$ and $T_{2,2XY8}$ versus temperature. Fitting

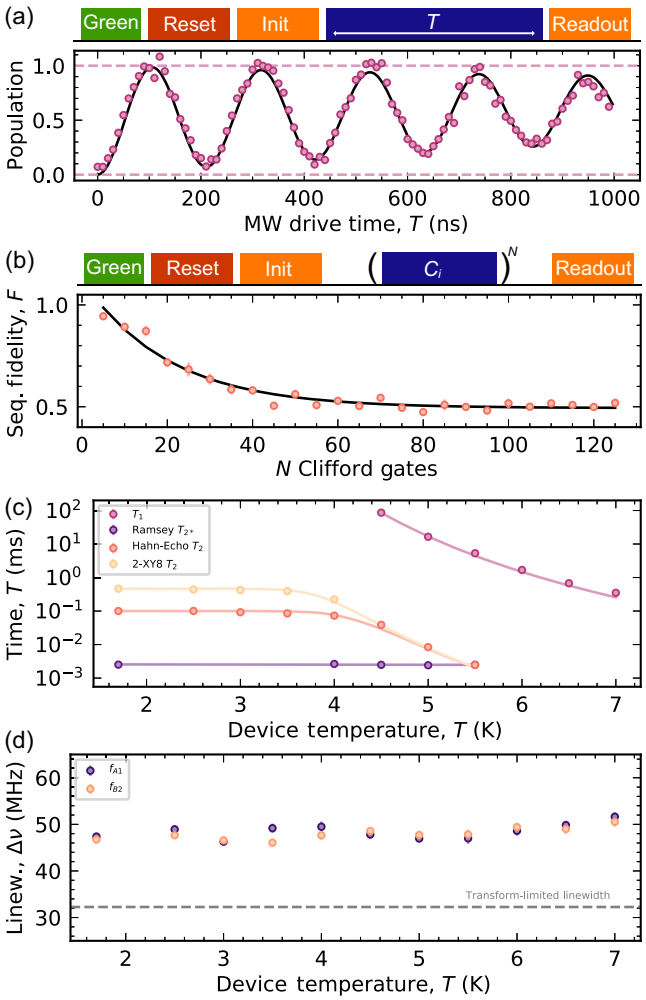

FIG. 5. Performance of the strained SnV center at 4 K. (a) Rabi oscillation of the SnV center, showing a gate fidelity of 97.7(5)%. (b) Randomized benchmarking at 4 K, showing an average gate fidelity of 95.7(3)%. (c) Temperature dependence of the spin decay time T_1^{spin}, dephasing times T_2^*, $T_{2,\mathrm{echo}}$, and $T_{2,2XY8}$. (d) ZPL linewidths of the two spin-conserving transitions ($A1$ and $B2$) with respect to the temperature, showing negligible broadening with the maximum linewidth below 52.0(8) MHz. The transform-limited linewidth is shown with a dashed line.

the same β factor in $T_2 \sim N^{\beta}$ using Hahn-echo and $XY4$ coherence times returns a value of 0.391(8) at 4 K and 0.014() at 4.5 K, indicating that the dominant decoherence mechanism becomes phonon-induced orbital transitions instead of the spin bath.

From Fig. 5(c), we notice a much lower dephasing time compared with the decay time T_1^{spin} [48]. This feature originates from the fact that only spin-flipping transitions between the lower and upper orbital branches drive T_1^{spin}, whereas T_2 is sensitive to dephasing by the spin-conserving transitions due to different precession frequencies in the orbital branches [23]. In our case, the phonon transitions are highly cycling due to the aligned magnetic field. Nevertheless, T_2^* at 4 K remains at 2.7(1) μs—comparable

to the 1.7 K value—and $T_{2,\mathrm{echo}}$ decreases only slightly to 74(2) μs, with $T_{2,2XY8}$ reaching the depolarization-limited T_2—223(10) μs. It is worth emphasizing that all of these are record-high values for all group IV spin qubits at 4 K to date.

To demonstrate the potential of the strained SnV center as a promising spin-photon interface at elevated temperature, we investigate the temperature dependence of the SnV optical coherence. As shown in Fig. 5(d), we observe that the ZPL linewidth remains unchanged for both $A1$ and $B2$ transitions up to 7 K with the maximum linewidth remaining below 52.0(8) MHz—only 60% higher than lifetime-limited values. In the future, modest Purcell enhancement of SnV emission rates with on-chip nanophotonics or microcavities can generate fully lifetime-limited photons suitable for efficient entanglement generation.

II. CONCLUSIONS

In this work, we demonstrate that SnV in strained diamond membranes is a promising platform for quantum technologies. We create simple heterostructures that leverage differences in thermal expansion to passively generate significant strain of 0.05% to 0.1% in diamond, enabling efficient, high-fidelity microwave control of the SnV spin. The presence of the strain also suppresses the phonon-mediated decay and improves the spin coherence of the SnV at 4 K, which greatly reduces the technological barrier for quantum networking applications. We reach a Rabi π gate fidelity of 99.36(9)% [97.7(5)%] with a randomized single-qubit gate fidelity of 97.7(1)% [95.7(3)%] at 1.7 K (4 K). Dynamical decoupling sequences allow the SnV spin coherence to reach 1.57(8) ms at 1.7 K and 223(10) μs at 4 K. In the future, this value can be further enhanced by generating higher strain through heterostructure optimization and/or additional active tuning. Our platform, derived from scalable diamond-membrane generation, is compatible with further on-chip integration, such as microwave coplanar waveguides, integrated photonics [32], and MEMS. Finally, 4 K cryostats are relatively affordable and less infrastructure intensive in comparison to cryogen-free 1.7 K and mK dilution-fridge systems. Therefore, the demonstrated spin-photon interface at 4 K can reduce barriers to widespread utilization and deployment of solid-state quantum technologies.

Note added. Recently, we became aware of another related manuscript [49].

ACKNOWLEDGMENTS

This work on strain engineering of group IV color centers is supported by the Air Force Office of Scientific Research under Grant No. FA9550-22-1-0518. This work acknowledges funding through Q-NEXT, supported by the U.S. Department of Energy, Office of Science, National Quantum Information Science Research Centers. The experiment receives support from the ERC Advanced Grant PEDESTAL (884745) and the EU Quantum Flagship 2D-SIPC. Membrane integration research is supported by NSF Grant No. AM-2240399. Diamond growth related efforts were supported by the U.S. Department of Energy, Office of Basic Energy Sciences, Materials Science and Engineering Division (N. D.). The membrane bonding work is supported by NSF Grant No. AM-2240399. This work made use of the Pritzker Nanofabrication Facility (Soft and Hybrid Nanotechnology Experimental Resource, NSF ECCS-2025633) and the Materials Research Science and Engineering Center (NSF DMR-2011854) at the University of Chicago. A. M. S. acknowledges support from EPSRC/NQIT, R. A. P. from the General Sir John Monash Foundation and G-research, J. A. M. from the Winton Program and EPSRC DTP, and C. P. M. from the EPSRC DTP. B. P. acknowledges funding from the European Union's Horizon 2020 research and innovation program under the Marie Skłodowska-Curie Grant Agreement No. 840968. The authors thank Eric I. Rosenthal, Abigail J. Stein, Hope Lee, Srujan Meesala, and Dorian Gangloff for insightful discussions and Haoxiong Yan and Ming-Han Chou for experimental help.

A. A. H., X. G., Z. L., T. L., N. D., and F. J. H. filed a provisional patent for the strain generation of bonded membranes.

[1] T. V. D. Sar, Z. H. Wang, M. S. Blok, H. Bernien, T. H. Taminiau, D. M. Toyli, D. A. Lidar, D. D. Awschalom, R. Hanson, and V. V. Dobrovitski, *Decoherence-protected quantum gates for a hybrid solid-state spin register*, Nature (London) **484**, 82 (2012).

[2] T. H. Taminiau, J. Cramer, T. van der Sar, V. V. Dobrovitski, and R. Hanson, *Universal control and error correction in multi-qubit spin registers in diamond*, Nat. Nanotechnol. **9**, 171 (2014).

[3] P.-J. Stas, Y. Q. Huan, B. Machielse, E. N. Knall, A. Suleymanzade, B. Pingault, M. Sutula, S. W. Ding, C. M. Knaut, D. R. Assumpcao, Y.-C. Wei, M. K. Bhaskar, R. Riedinger, D. D. Sukachev, H. Park, M. Lončar, D. S. Levonian, and M. D. Lukin, *Robust multi-qubit quantum network node with integrated error detection*, Science **378**, 557 (2022).

[4] M. Pompili, S. L. N. Hermans, S. Baier, H. K. C. Beukers, P. C. Humphreys, R. N. Schouten, R. F. L. Vermeulen, M. J. Tiggelman, L. dos Santos Martins, B. Dirkse, S. Wehner, and R. Hanson, *Realization of a multinode quantum network of remote solid-state qubits*, Science **372**, 259 (2021).

[5] S. L. Hermans, M. Pompili, H. K. Beukers, S. Baier, J. Borregaard, and R. Hanson, *Qubit teleportation between non-neighbouring nodes in a quantum network*, Nature (London) **605**, 663 (2022).

[6] G. Kucsko, P. C. Maurer, N. Y. Yao, M. Kubo, H. J. Noh, P. K. Lo, H. Park, and M. D. Lukin, *Nanometre-scale thermometry in a living cell*, Nature (London) **500**, 54 (2013).

[7] F. Shi, F. Kong, P. Zhao, X. Zhang, M. Chen, S. Chen, Q. Zhang, M. Wang, X. Ye, Z. Wang, Z. Qin, X. Rong, J. Su, P. Wang, P. Z. Qin, and J. Du, *Single-DNA electron spin resonance spectroscopy in aqueous solutions*, Nat. Methods **15**, 697 (2018).

[8] E. N. Knall, C. M. Knaut, R. Bekenstein, D. R. Assumpcao, P. L. Stroganov, W. Gong, Y. Q. Huan, P.-J. Stas, B. Machielse, M. Chalupnik *et al.*, *Efficient source of shaped single photons based on an integrated diamond nanophotonic system*, Phys. Rev. Lett. **129**, 053603 (2022).

[9] M. K. Bhaskar, D. D. Sukachev, A. Sipahigil, R. E. Evans, M. J. Burek, C. T. Nguyen, L. J. Rogers, P. Siyushev, M. H. Metsch, H. Park *et al.*, *Quantum nonlinear optics with a germanium-vacancy color center in a nanoscale diamond waveguide*, Phys. Rev. Lett. **118**, 223603 (2017).

[10] J. A. Martínez, R. A. Parker, K. C. Chen, C. M. Purser, L. Li, C. P. Michaels, A. M. Stramma, R. Debroux, I. B. Harris, M. H. Appel *et al.*, *Photonic indistinguishability of the tin-vacancy center in nanostructured diamond*, Phys. Rev. Lett. **129**, 173603 (2022).

[11] Y. Narita, P. Wang, K. Ikeda, K. Oba, Y. Miyamoto, T. Taniguchi, S. Onoda, M. Hatano, and T. Iwasaki, *Multiple tin-vacancy centers in diamond with nearly identical photon frequency and linewidth*, Phys. Rev. Appl. **19**, 024061 (2023).

[12] A. E. Rugar, C. Dory, S. Aghaeimeibodi, H. Lu, S. Sun, S. D. Mishra, Z.-X. Shen, N. A. Melosh, and J. Vuckovic, *Narrow-linewidth tin-vacancy centers in a diamond waveguide*, ACS Photonics **7**, 2356 (2020).

[13] N. H. Wan, T.-J. Lu, K. C. Chen, M. P. Walsh, M. E. Trusheim, L. De Santis, E. A. Bersin, I. B. Harris, S. L. Mouradian, I. R. Christen, E. S. Bielejec, and D. Englund, *Large-scale integration of artificial atoms in hybrid photonic circuits*, Nature (London) **583**, 226 (2020).

[14] J. Görlitz, D. Herrmann, G. Thiering, P. Fuchs, M. Gandil, T. Iwasaki, T. Taniguchi, M. Kieschnick, J. Meijer, M. Hatano, A. Gali, and C. Becher, *Spectroscopic investigations of negatively charged tin-vacancy centres in diamond*, New J. Phys. **22**, 013048 (2020).

[15] T. Iwasaki, Y. Miyamoto, T. Taniguchi, P. Siyushev, M. H. Metsch, F. Jelezko, and M. Hatano, *Tin-vacancy quantum emitters in diamond*, Phys. Rev. Lett. **119**, 253601 (2017).

[16] L. De Santis, M. E. Trusheim, K. C. Chen, and D. R. Englund, *Investigation of the stark effect on a centrosymmetric quantum emitter in diamond*, Phys. Rev. Lett. **127**, 147402 (2021).

[17] S. Aghaeimeibodi, D. Riedel, A. E. Rugar, C. Dory, and J. Vučković, *Electrical tuning of tin-vacancy centers in diamond*, Phys. Rev. Appl. **15**, 064010 (2021).

[18] C. Hepp, T. Müller, V. Waselowski, J. N. Becker, B. Pingault, H. Sternschulte, D. Steinmüller-Nethl, A. Gali, J. R. Maze, M. Atatüre, and C. Becher, *Electronic structure of the silicon vacancy color center in diamond*, Phys. Rev. Lett. **112**, 036405 (2014).

[19] A. Sipahigil, R. E. Evans, D. D. Sukachev, M. J. Burek, J. Borregaard, M. K. Bhaskar, C. T. Nguyen, J. L. Pacheco, H. A. Atikian, C. Meuwly, R. M. Camacho, F. Jelezko, E. Bielejec, H. Park, M. Lončar, and M. D. Lukin, *An integrated diamond nanophotonics platform for quantum-optical networks*, Science **354**, 847 (2016).

[20] K. D. Jahnke, A. Sipahigil, J. M. Binder, M. W. Doherty, M. Metsch, L. J. Rogers, N. B. Manson, M. D. Lukin, and F. Jelezko, *Electron-phonon processes of the silicon-vacancy centre in diamond*, New J. Phys. **17**, 043011 (2015).

[21] J. N. Becker, B. Pingault, D. Groß, M. Gündoğan, N. Kukharchyk, M. Markham, A. Edmonds, M. Atatüre, P. Bushev, and C. Becher, *All-optical control of the silicon-vacancy spin in diamond at millikelvin temperatures*, Phys. Rev. Lett. **120**, 053603 (2018).

[22] D. D. Sukachev, A. Sipahigil, C. T. Nguyen, M. K. Bhaskar, R. E. Evans, F. Jelezko, and M. D. Lukin, *Silicon-vacancy spin qubit in diamond: A quantum memory exceeding 10 ms with single-shot state readout*, Phys. Rev. Lett. **119**, 223602 (2017).

[23] S. Meesala, Y. I. Sohn, B. Pingault, L. Shao, H. A. Atikian, J. Holzgrafe, M. Gündoğan, C. Stavrakas, A. Sipahigil, C. Chia, R. Evans, M. J. Burek, M. Zhang, L. Wu, J. L. Pacheco, J. Abraham, E. Bielejec, M. D. Lukin, M. Atatüre, and M. Lončar, *Strain engineering of the silicon-vacancy center in diamond*, Phys. Rev. B **97**, 205444 (2018).

[24] Y. I. Sohn, S. Meesala, B. Pingault, H. A. Atikian, J. Holzgrafe, M. Gündoğan, C. Stavrakas, M. J. Stanley, A. Sipahigil, J. Choi, M. Zhang, J. L. Pacheco, J. Abraham, E. Bielejec, M. D. Lukin, M. Atatüre, and M. Lončar, *Controlling the coherence of a diamond spin qubit through its strain environment*, Nat. Commun. **9**, 2012 (2018).

[25] M. E. Trusheim *et al.*, *Transform-limited photons from a coherent tin-vacancy spin in diamond*, Phys. Rev. Lett. **124**, 023602 (2020).

[26] R. Debroux, C. P. Michaels, C. M. Purser, N. Wan, M. E. Trusheim, J. A. Martínez, R. A. Parker, A. M. Stramma, K. C. Chen, L. D. Santis, E. M. Alexeev, A. C. Ferrari, D. Englund, D. A. Gangloff, and M. Atatüre, *Quantum control of the tin-vacancy spin qubit in diamond*, Phys. Rev. X **11**, 041041 (2021).

[27] X. Guo, N. Delegan, J. C. Karsch, Z. Li, T. Liu, R. Shreiner, A. Butcher, D. D. Awschalom, F. J. Heremans, and A. A. High, *Tunable and transferable diamond membranes for integrated quantum technologies*, Nano Lett. **21**, 10392 (2021).

[28] Y. K. Siew, G. Sarkar, X. Hu, J. Hui, A. See, and C. T. Chua, *Thermal curing of hydrogen silsesquioxane*, J. Electrochem. Soc. **147**, 335 (2000).

[29] See Supplemental Material at http://link.aps.org/supplemental/10.1103/PhysRevX.13.041037 for additional theoretical calculation, device fabrication and supporting measurements.

[30] C. Dang, J.-P. Chou, B. Dai, C.-T. Chou, Y. Yang, R. Fan, W. Lin, F. Meng, A. Hu, J. Zhu, J. Han, A. M. Minor, J. Li, and Y. Lu, *Achieving large uniform tensile elasticity in microfabricated diamond*, Science **371**, 76 (2021).

[31] A. Butcher, X. Guo, R. Shreiner, N. Delegan, K. Hao, P. J. Duda, D. D. Awschalom, F. J. Heremans, and A. A. High, *High-Q nanophotonic resonators on diamond membranes using templated atomic layer deposition of* TiO_2, Nano Lett. **20**, 4603 (2020).

[32] X. Guo, M. Xie, A. Addhya, A. Linder, U. Zvi, T. D. Deshmukh, Y. Liu, I. N. Hammock, Z. Li, C. T. DeVault, A. Butcher, A. P. Esser-Kahn, D. D. Awschalom, N. Delegan, P. C. Maurer, F. J. Heremans, and A. A. High, *Direct-bonded diamond membranes for heterogeneous quantum and electronic technologies*, arXiv:2306.04408.

[33] G. Thiering and A. Gali, *Ab initio magneto-optical spectrum of group-iv vacancy color centers in diamond*, Phys. Rev. X **8**, 021063 (2018).

[34] A. E. Rugar, S. Aghaeimeibodi, D. Riedel, C. Dory, H. Lu, P. J. McQuade, Z.-X. Shen, N. A. Melosh, and J. Vučković, *Quantum photonic interface for tin-vacancy centers in diamond*, Phys. Rev. X **11**, 031021 (2021).

[35] R. A. Parker, J. A. Martínez, K. C. Chen, A. M. Stramma, I. B. Harris, C. P. Michaels, M. E. Trusheim, M. H. Appel, C. M. Purser, W. G. Roth, D. Englund, and M. Atatüre, *A diamond nanophotonic interface with an optically accessible deterministic electronuclear spin register*, arXiv:2305.18923.

[36] M. K. Bhaskar, R. Riedinger, B. Machielse, D. S. Levonian, C. T. Nguyen, E. N. Knall, H. Park, D. Englund, M. Lončar, D. D. Sukachev, and M. D. Lukin, *Experimental demonstration of memory-enhanced quantum communication*, Nature (London) **580**, 60 (2020).

[37] P. Fuchs, T. Jung, M. Kieschnick, J. Meijer, and C. Becher, *A cavity-based optical antenna for color centers in diamond*, APL Photonics **6** (2021).

[38] C. Güney Torun, P.-I. Schneider, M. Hammerschmidt, S. Burger, J. H. Munns, and T. Schröder, *Optimized diamond inverted nanocones for enhanced color center to fiber coupling*, Appl. Phys. Lett. **118**, 234002 (2021).

[39] K. Kuruma, B. Pingault, C. Chia, D. Renaud, P. Hoffmann, S. Iwamoto, C. Ronning, and M. Lončar, *Coupling of a single tin-vacancy center to a photonic crystal cavity in diamond*, Appl. Phys. Lett. **118**, 230601 (2021).

[40] N. Tomm, A. Javadi, N. O. Antoniadis, D. Najer, M. C. Löbl, A. R. Korsch, R. Schott, S. R. Valentin, A. D. Wieck, A. Ludwig *et al.*, *A bright and fast source of coherent single photons*, Nat. Nanotechnol. **16**, 399 (2021).

[41] D. Riedel, I. Söllner, B. J. Shields, S. Starosielec, P. Appel, E. Neu, P. Maletinsky, and R. J. Warburton, *Deterministic enhancement of coherent photon generation from a nitrogen-vacancy center in ultrapure diamond*, Phys. Rev. X **7**, 031040 (2017).

[42] M. Ruf, M. J. Weaver, S. B. van Dam, and R. Hanson, *Resonant excitation and Purcell enhancement of coherent nitrogen-vacancy centers coupled to a Fabry-Perot microcavity*, Phys. Rev. Appl. **15**, 024049 (2021).

[43] B. Pingault, D. D. Jarausch, C. Hepp, L. Klintberg, J. N. Becker, M. Markham, C. Becher, and M. Atatüre, *Coherent control of the silicon-vacancy spin in diamond*, Nat. Commun. **8**, 15579 (2017).

[44] S. Sangtawesin, B. L. Dwyer, S. Srinivasan, J. J. Allred, L. V. H. Rodgers, K. De Greve, A. Stacey, N. Dontschuk, K. M. O'Donnell, D. Hu *et al.*, *Origins of diamond surface noise probed by correlating single-spin measurements with surface spectroscopy*, Phys. Rev. X **9**, 031052 (2019).

[45] G. De Lange, Z.-H. Wang, D. Riste, V. Dobrovitski, and R. Hanson, *Universal dynamical decoupling of a single solid-state spin from a spin bath*, Science **330**, 60 (2010).

[46] A. M. Souza, G. A. Alvarez, and D. Suter, *Robust dynamical decoupling for quantum computing and quantum memory*, Phys. Rev. Lett. **106**, 240501 (2011).

[47] K. Kuruma, B. Pingault, C. Chia, M. Haas, G. D. Joe, D. R. Assumpcao, S. W. Ding, C. Jin, C. J. Xin, M. Yeh, N. Sinclair, and M. Lončar, *Engineering phonon-qubit interactions using phononic crystals*, arXiv:2310.06236.

[48] L. J. Rogers, K. D. Jahnke, M. H. Metsch, A. Sipahigil, J. M. Binder, T. Teraji, H. Sumiya, J. Isoya, M. D. Lukin, P. Hemmer, and F. Jelezko, *All-optical initialization, readout, and coherent preparation of single silicon-vacancy spins in diamond*, Phys. Rev. Lett. **113**, 263602 (2014).

[49] E. I. Rosenthal, C. P. Anderson, H. C. Kleidermacher, A. J. Stein, H. Lee, J. Grzesik, G. Scuri, A. E. Rugar, D. Riedel, S. Aghaeimeibodi *et al.*, *Microwave spin control of a tin-vacancy qubit in diamond*, Phys. Rev. X **13**, 031022 (2023).